

An automatic method to analyze the Capacity-Voltage and Current-Voltage curves of a sensor

Pablo Matorras Cuevas

CERN summer student, 2017.

Supervisor: Marcos Fernandez Garcia.

(Dated: August 30, 2017)

An automatic method to perform Capacity versus voltage analysis for all kind of silicon sensor is provided. It successfully calculates the depletion voltage to unirradiated and irradiated sensors, and with measurements with outliers or reaching breakdown. It is built using C++ and using ROOT trees with an analogous skeleton as TRICS, where the data as well as the results of the fits are saved, to make further analysis.

I. INTRODUCTION

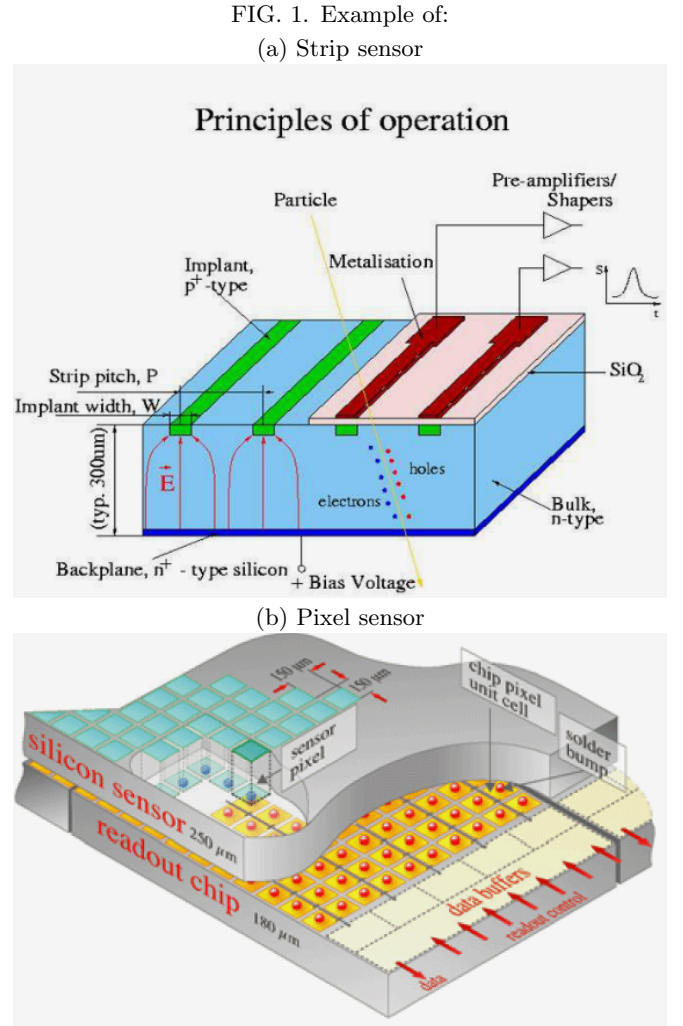
CERN RD-50 is a collaboration which includes more than 50 institutes from more than 42 countries, with a total of around 300 members [1]. Its main target of the collaboration is to develop silicon sensors that are able to operate in the High Luminosity LHC phase [2]. In this phase, LHC luminosity will be increased from around a maximum luminosity of $\sim 300 fb^{-1}$ in 2020 (Currently around $\sim 30 fb^{-1}$) to $\sim 3000 fb^{-1}$ by 2030 [3, 4]. In this scenario, silicon sensors close to the interaction point will have to withstand a radiation fluence of $1 - 2 \times 10^{16} n_{eq}/cm^2$ [2, 5].

Current detectors nowadays can not withstand this fluence. More radiation hard (no mas precisos) devices are needed to be developed.

Traditionally, two types of sensors have been especially important. Those are the strip and the pixel sensors. Strip sensors were first introduced for the study of charm quarks [6]. It operates typically with a configuration of a n-type bulk, with a p^+ implant, to where a bias voltage is applied, as shown in Fig 1 (a). They are characterized by a high spatial resolution and good efficiency for a relatively low cost compared to other sensors, although because a reconstruction of the track is required, its use becomes difficult when distinguishing several tracks. They are used in tracker detectors [1, 7].

Pixel detectors where developed later than strip sensors, and are silicon segments of a highly granular diode matrix, with a readout with the same geometry, and connections done via bonding (schematic representation shown in Fig 1 (b)). Unlike strip sensors, a true 2D resolution is obtained for pixel sensors, but with a higher cost than the strip sensors. This type of sensors are currently used in all LHC experiments (ATLAS, CMS, ALICE and LHCb) [1, 7].

New types of sensors are being developed, with a smaller thickness, different materials, concentration, or different distributions [1]. In this terms, it is especially promising the use of 3D sensors [5], where the electrons



penetrate the silicon substrate, obtaining therefore a 3-Dimensional image [8]. This has been successfully implemented as a layer in ATLAS [9] and it is currently considered to be also implemented in CMS [10].

II. SENSOR CHARACTERIZATION

At SSD [1, 2], several semiconductor characterization techniques are put in place:

A. TCT technique

TCT or transit current technique uses a laser pulse to induce charge carriers inside the sensor to simulate the pass of a particle. Time resolved current is calculated with the Ramo theorem (Equation 1) where \vec{v} is the drift velocity for an Electric field E , and \vec{E}_W is the weighing field. [1, 7]

$$I(t) = -q \cdot \vec{v} \cdot \vec{E}_W \quad (1)$$

With the laboratory set up, two different wavelengths can be used, red ($\lambda = 640$ nm) and infrared ($\lambda = 1064$ nm), where because of the penetration depth is rather different ($\sim 10\mu m$ for red, 1 mm for IR), carrier distributions will be different depending on the type of TCT being produced [11]. Also, the set up is built so that the incident laser can be from the top of the sensor, or its bottom, so that a more precise knowledge of the boundaries can be acquired.

Another method that can be used is what's called Edge-TCT[11], where the beam is injected from the side (width of the beam smaller than the thickness of the detector). This method allows to profile several characteristics of the detector as a function of depth, like the charge collection or even the drift velocity [11].

B. CV-IV measurements

In addition to the TCT technique, other measurements can be done to characterize the sensor. These are the case of the Capacity-Voltage (CV) and the Current-Voltage (IV) measurements. The main property obtained from them is the depletion voltage, which is the voltage at which all the sensor is depleted, with an importance that arises from the fact that sensors in LHC are expected to work at full depletion [7]. This value can be spotted directly from the change in the curvature for the IV measurements, or from the curve of $C^{-2}V$ representation.

Other important variables that can be calculated from these measurements are the effective doping concentration, the end capacitance, and the thickness.

The effective doping concentration denotes the number of carriers (mainly produced in the doping) per unit volume, whereas the end capacitance is defined as the capacitance of the sensor if it is completely depleted. It

is defined as the capacity for a voltage $V = 1.2 \times V_{dep}$ [12]. Finally, the depletion depth shows the depth up which the detector is depleted. It can be calculated in Equation 2

$$N_{eff} = \frac{2}{A\epsilon\epsilon_0 q_0} \frac{1}{\frac{d(1/C^2)}{dV}} \quad (2)$$

If the effective doping concentration and the thickness are known, all the other variables can be expressed in terms of it [1, 7]:

$$V_{dep} = \frac{q_0}{2\epsilon\epsilon_0} |N_{eff}| d^2 \quad (3)$$

$$w(V) = \sqrt{\frac{2\epsilon\epsilon_0}{q_0 |N_{eff}|} V} \quad (4)$$

Where from eq 3 the depletion voltage, and from eq. 4 the depletion depth are calculated. q_0 is the electron charge and $\epsilon\epsilon_0$ the silicon relative permittivity and absolute (vacuum) permittivity. In addition to that, The capacity can be expressed either in terms of the voltage as shown in Equation 5 or in terms of the depletion depth 6 For a detector area A:

$$C(U) = A \cdot \sqrt{\frac{q_0\epsilon\epsilon_0}{2V}} \quad (5)$$

$$C(w) = \frac{\epsilon\epsilon_0 A}{w} \quad (6)$$

Also, the detector thickness can be calculated from Eq 7.

$$d = \frac{\epsilon\epsilon_0}{C_{end}} \quad (7)$$

C. Radiation Damage

In LHC, silicon detectors suffer a big amount of radiation ($1 - 2 \times 10^{16} n_{eq}cm^2$). This radiation is capable of modifying the properties of the sensors. The most remarkable case is the type inversion, in which a n-type sensor can turn into a p-type sensor, as the effective doping concentration changes from positive to negative. Also, its depletion voltage increases significantly, so that the voltage necessary for the detectors to be used in the collider conditions is higher [1, 4, 7, 11].

In order to radiation damage to be studied in the laboratory, the same TCT and CVIV measurements are done to the same sensors unirradiated and irradiated. The irradiation takes place mainly in CERN if protons are used [13], or in Ljubljana in case of neutron irradiation [14].

III. CVIV_TREE PROGRAM

In order to study CV-IV profiles, it is required to make an analysis to both the current-voltage and the $1/\text{Capacity}^2$ curves. In order to achieve this, a new analysis software is created. The program that reads the .cv or .iv files created where a measurement was taken, and saves the data into a ROOT tree.

This tree has two branches, cv and iv, where data will be saved depending of the type of measurement done. Inside each branch, multiple leafs are created with the data in the header (date, Temperature, user, fluence...) and IV or CV measurements saved as vector.

Each branch is mapped as a class, therefore there are two classes, TIV and TCV, with both a header and a body. the TIV class is in charge of creating all the variables and vectors that are required to save a .iv file into the iv branch of the tree. Similar procedure is followed by the TCV class, plus additional variables calculated from the fit that will be explained in Section IV.

The program is compiled and is run from the linux shell. In an Intel Pentium dualcore the analysis speed is approximately ~ 200 files/s, outputting a ROOT tree with both data information and results of the tree, as well as a pdf with the result of the Fit in $1/C^2$ shown in Section IV.

Once the Tree is created, it can be interactively analyzed by using ROOT, where all the variables can be plotted or scanned using the desired conditions.

IV. FIT IN $1/C^2$

A. First estimation

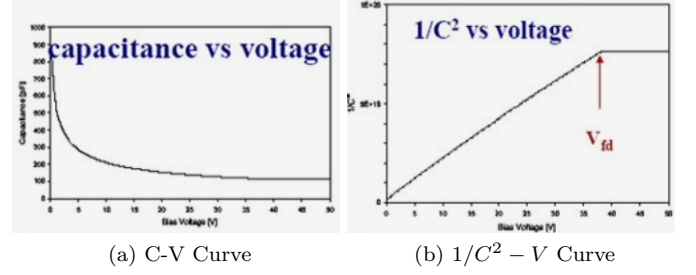
In order to calculate the depletion voltage, it is useful to study the behaviour of the inverse of the capacity squared which is linear in voltage. An example of an ideal curve is shown in Figure 2, where as it can be seen the depletion voltage is calculated as the intersection of two straight lines fitted simultaneously to the rising and to the plateau.

This method, that has been proven to be properly working, has been implemented in an automatic way, following the next steps for each of the cv files.

1. Points that are in breakdown are neglected. For doing so, breakdown is assumed to happen when $k_{bd} > 4$ [12] being defined as shown in Eq 8 for each i th element of Voltage or Current.

$$k_{bd} = \frac{\Delta I}{\Delta V} \cdot \frac{V}{I} = \frac{I[ii] - I[ii-1]}{V[ii] - V[ii-1]} \cdot \frac{V[ii]}{I[ii]} \quad (8)$$

FIG. 2. Ideal curve of an undepleted sensor for:



2. From the $1/C^2$ distribution, calculate the mean and the RMS of the distribution.
3. Estimate the last valid point for fitting the slope, and the first point for fitting the plateau. To take into account the asymmetry of the distribution, the first fit point (end of the first fit range) we have found that can be taken to be mean-rms, whereas the other is mean+0.15rms.
4. From the first and the second range, calculate two linear fits from where the depletion voltage is calculated as its intersection.

Once the depletion voltage is obtained, the effective doping concentration can be calculated using Equation 2, with $d(1/C^2)/dV$ is the slope of the first line. Finally, the thickness can be calculated from Eq 7. An output file in pdf is created where both lines from the fit are shown with the original data, with the depletion voltage calculated as:

$$V_{dep} = \frac{a_1 - a_2}{b_2 - b_1} \quad (9)$$

For the results of the fits of both lines, defined as $y = a_i + b_i x$ where a_i and b_i are the intercept and slope of the straight lines respectively. In addition to that, an estimated error can be propagated, as shown in 10:

$$\delta V_{dep}[0] = V_{dep}[0] \sqrt{\left(\frac{\sqrt{\delta a_1^2 + \delta a_2^2}}{a_1 - a_2} \right)^2 + \left(\frac{\sqrt{\delta b_1^2 + \delta b_2^2}}{b_1 - b_2} \right)^2} \quad (10)$$

Where δa_i and δb_i are the errors of a_i and b_i . This estimated error is also shown with a dashed line. Also, the value of the end capacitance, previously calculated is shown, together with the temperature, date, and χ^2 for both fits. An example fit is shown in Fig 3 for a typical diode. It is not the case for the second fit displayed (Fig 4) for a diode where breakdown is obtained before the CV measurement is finished.

Note that whereas for the second fit the value has a reasonable value, it does not for the first case. This arises from the fact that having estimated the error in the Capacitance, if the error of $1/C^2$ is calculated (Section A),

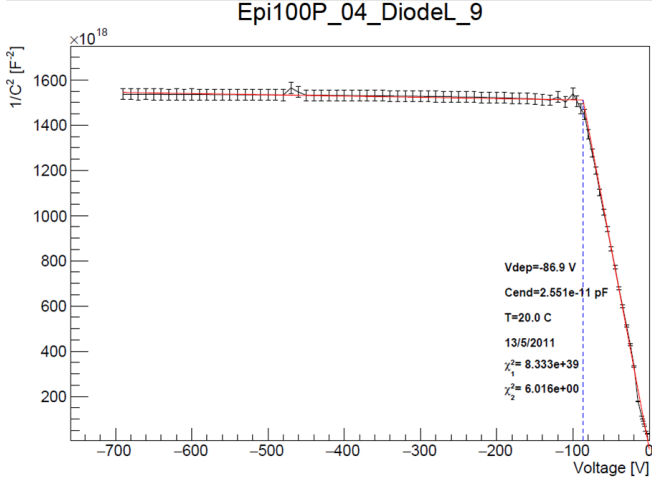


FIG. 3. Example of a fit calculated for a typical diode CV curve.

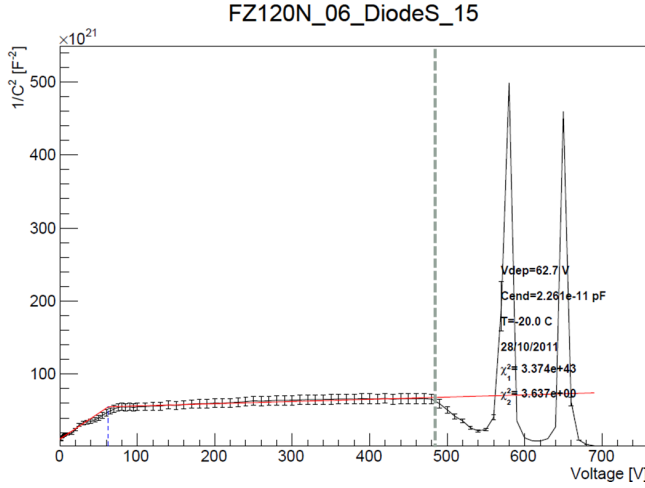


FIG. 4. Example of a fit calculated for a diode that reaches the breakdown. The dashed line on the left of the image shows where the breakdown is calculated to be.

it will depend on the inverse of the Capacitance cubic, and therefore, if error bars are taken into account for the fit, it will be forced to pass through the first values, which are known empirically to have a higher systematic error. Because of this reason, the first fit was calculated supposing equal weights.

B. Data filtering

In order to obtain a better result, several algorithms are implemented if required:

1. A five point stencil formula [15] (shown in Eq 11) is calculated for the values in the first range, so that if its sign is negative, all the points before the derivative changes to positive are neglected. This is good to discard measurements where $1/C^2$ first

drops and then starts increasing, as shown in Fig 5.

$$f'(x) \approx \frac{-f(x+2h) + 8f(x+h) - 8f(x-h) + f(x-2h)}{12h} \quad (11)$$

2. For outlier points to discard clear outliers like the measurements around 260 V in Fig 6 which are 1.5 bigger than the previous and the posterior point are neglected.
3. For drops of $1/C^2$, points which are smaller than 0.7 the value of $1/C^2$ at the start of the second range are neglected. This behaviour is shown in Fig 6

Once this filter is done, the procedure explained in section IV A is repeated.

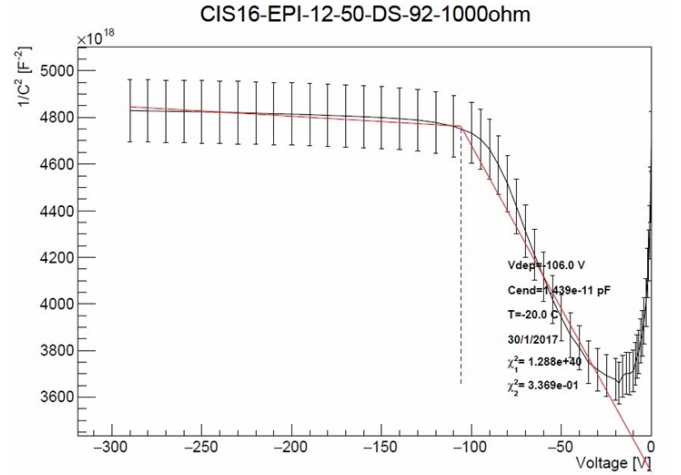


FIG. 5. Example of a fit calculated for a diode whose $1/C^2$ measurement start decreasing and then increases

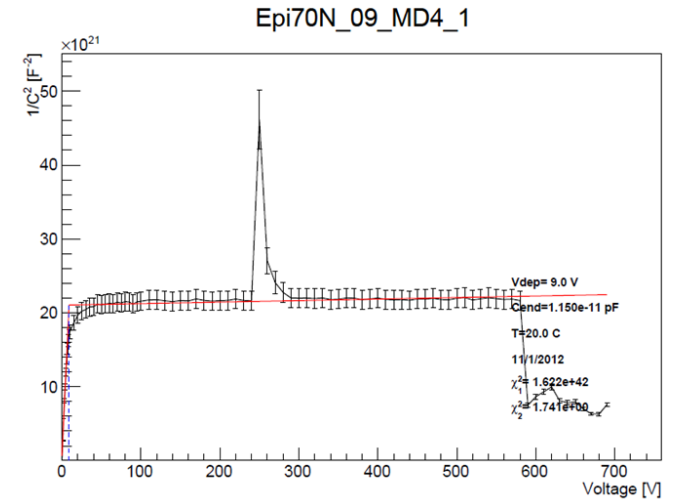
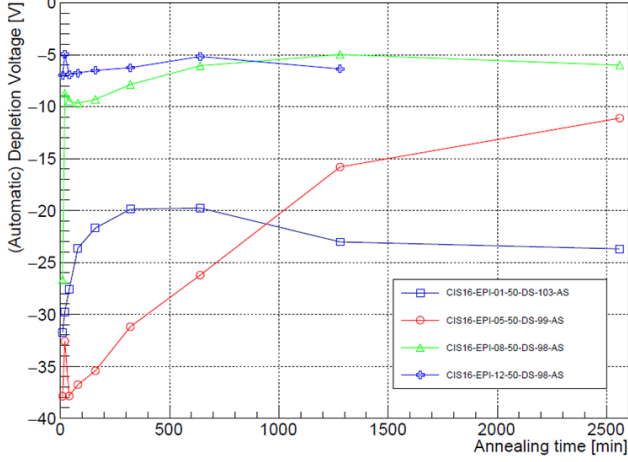


FIG. 6. Example of a fit calculated for a diode whose $1/C^2$ measurement has both individual outliers, and a sudden decrease of the values.

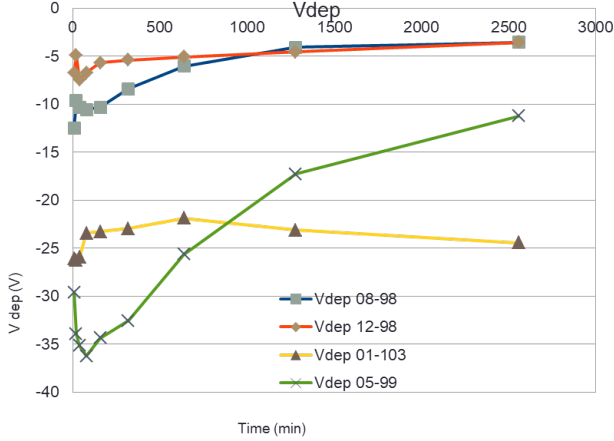
C. Comparison with a manual fit

In order to test the performance of the program, the depletion voltage obtained with this method was compared to the calculated to the calculated values using an estimation by eye of the fitting ranges. The compared results are shown in Figure 7.

FIG. 7.



(a) Depletion voltage obtained using the automatic fitting algorithym



(b) Depletion voltage obtained manually by M. Thalmayr

V. LIMITATIONS AND FURTHER STEPS

Although it is remarkable the few differences of performing the analysis using TCV to doing them manually, there are still some limitations to the performance of it. The most clear is those sensor measurements where although there is a increase of the depletion voltage, it is not linear and, thus, a poor linear fit is obtained. This is shown in Figure 8. Different solutions were thought to attempt to overcome this issue, such as fitting to higher

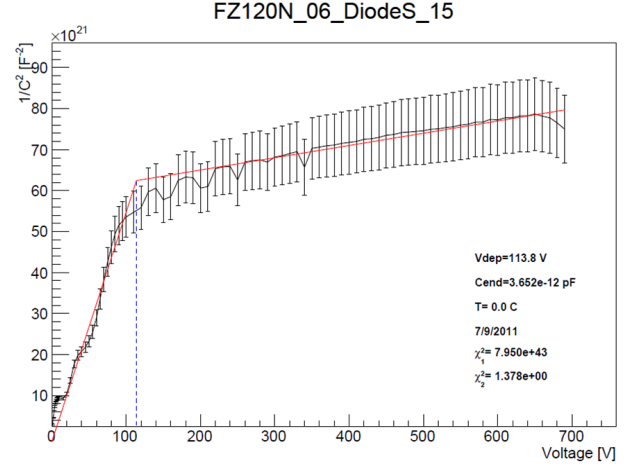


FIG. 8. Example of a fit calculated for a sensor measurement where the ramp up is not linear.

polynomials and other functions, but not a satisfactory result was obtained.

Another way thought was to calculate the depletion voltage from the change in the derivative slope. In this way, the Five point stencil was extended to all the range. This took considerable efforts to take into account the fact that the voltage step (de difference of the value of a voltage and the previous) was not always symmetrical. The issue was solved both making a interpolation of the points using a Cubic Spline so that the five point stencil can be directly calculated; and also simply by applying a 3 or 2 point derivative in those cases where the intervals where asymmetrical, being the interpolation derivative smoother.

However, looking at the derivative distribution for both cases, there was not found a more precise way to calculate, as if the derivative is shown in an histogram (Fig 9), although for the plateau the values accumulate in the same point, for the ramp up there is a big variation. And if the calculation is desired to be done over the variation of the derivative with respect to the voltage, the problem ends with the same problem as from calculating it from the original value (see Fig 10).

Nevertheless, by looking at both Fig 9 and 10 it can be seen that another method independent to the original could be calculated, either from the histogram, calculating the mean of the values around zero and with a value clearly higher than it, or by looking at the shape of the derivative.

An additional step that can be implemented is to make the correction to resistance in series to the one in parallel, using the conversion shown in Eq 12 [16].

$$C_s = \frac{1 + \omega^2 R_p^2 C_p^2}{\omega^2 R_p^2 C_p^2} \quad (12)$$

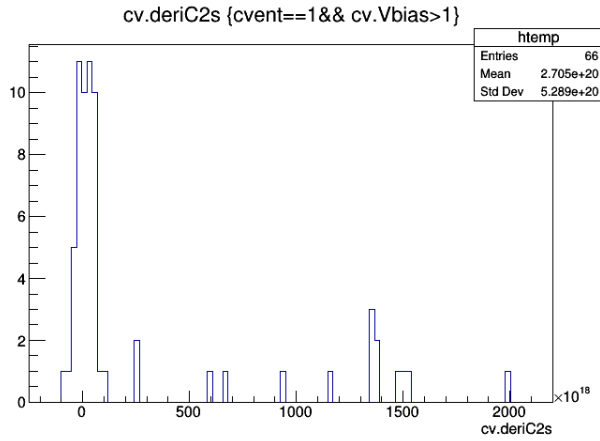


FIG. 9. Histogram of the values of the derivative of $1/C^2$.

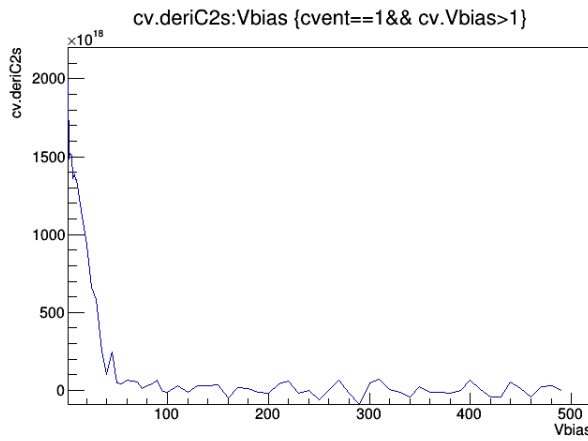


FIG. 10. Values of the derivative of $1/C^2$ with respect to the bias voltage.

This value has been implemented to the code, as well as in $1/C^2$, so that the correction should be easy to be fixed.

VI. CONCLUSIONS

Given the speed of the fit together with the quality of the obtained values, the program can be regarded as valid, at least to get a quick estimate, (looking at the similarities between Fig 7 (a) and (b)), and the fact that the results are saved in a tree where one can distinguish between each event, or include various conditions or cut-offs. There is still clear room to improvements, to be extended to other independent methods to calculate the depletion voltage, such as from its derivative, or from the I-V curve: as well as the possibility of being merged with TRACS in order to create a general program that can be used to perform fast TCT or CVIV analysis in a fast and efficient way.

Appendix A: Error calculation

- The error in the voltage has been assumed to be zero.
- The error in the capacitance is taken to be 0.2 pF
- The error in $1/C^2$ is calculated to be $\delta(1/C^2) = \frac{2\delta C}{C^3}$

-
- [1] M. Fernndez, M. Moll, “Workshop on the characterization of irradiated silicon sensors & effects of radiation on solid state particle detector performance,” (2017).
 - [2] G. Casse, Journal of Instrumentation **10**, C05020 (2015).
 - [3] D. Bortoletto, Journal of Instrumentation **10**, C08016 (2015).
 - [4] P. Vankov, in *EPJ Web of Conferences*, Vol. 28 (EDP Sciences, 2012) p. 12069.
 - [5] J. Lange, S. Grinstein, M. Manna, G. Pellegrini, D. Quirion, S. Terzo, and D. V. Furelos, arXiv preprint arXiv:1707.01045 (2017).
 - [6] J. Kemmer, E. Belau, R. Klanner, G. Lutz, and B. Hyams, Proc. Silicon Detectors for High Energy Physics, 195 (1981).
 - [7] H. Spieler, *Semiconductor Detector Systems*, Series on Semiconductor Science and Technology (OUP Oxford, 2005).
 - [8] C. Da Via, M. Boscardin, G.-F. Dalla Betta, G. Darbo, C. Fleta, C. Gemme, P. Grenier, S. Grinstein, T.-E. Hansen, J. Hasi, *et al.*, Nuclear Instruments and Methods in Physics Research Section A: Accelerators, Spectrometers, Detectors and Associated Equipment **694**, 321 (2012).
 - [9] G. Darbo, Journal of Instrumentation **10**, C05001 (2015).
 - [10] W. Adam, T. Bergauer, E. Brondolin, M. Dragicevic, Friedl, *et al.*, The European Physical Journal C **77**, 567 (2017).
 - [11] I. Mandić, V. Cindro, A. Gorišek, G. Kramberger, M. Mikuz, and M. Zavrtanik, Journal of Instrumentation **10**, P08004 (2015).
 - [12] G.-F. Dalla Betta, N. Ayllon, M. Boscardin, M. Hoeflerkamp, S. Mattiazzi, H. McDuff, R. Mendicino, M. Povoli, S. Seidel, D. Sultan, *et al.*, Journal of Instrumentation **11**, P09006 (2016).
 - [13] M. Glaser, F. Ravotti, and M. Moll, in *Radiation and Its Effects on Components and Systems, 2005. RADECS 2005. 8th European Conference on* (IEEE, 2005) pp. P15–1.
 - [14] M. Moll, E. Fretwurst, G. Lindström, *et al.*, Nuclear Instruments and Methods in Physics Research Section A: Accelerators, Spectrometers, Detectors and Associated Equipment **426**, 87 (1999).

- [15] C. Grossmann, H. Roos, and M. Stynes, *Numerical Treatment of Partial Differential Equations*, Universitext (Springer Berlin Heidelberg, 2007).
- [16] M. Moll, *Radiation damage in silicon particle detectors: Microscopic defects and macroscopic properties*, Tech. Rep. (DESY, 1999).